Achieving high strain rate superplasticity in an Al–Li–Mg alloy through equal channel angular extrusion

R. Kaibyshev*[1], K. Shipilova[1], F. Musin[1] and Y. Motohashi[2]

An Al–Li–Mg–Sc–Zr alloy was fabricated by an ingot metallurgy technique and subjected to intense plastic straining through equal channel angular extrusion at three different temperatures, 240, 325 and 400°C. The superplastic properties and microstructure evolution of the alloy were examined in tension in the temperature interval 250–500°C at strain rates ranging from $1{\cdot}4 \times 10^{-5}$ to $1{\cdot}4\ s^{-1}$. Superior superplastic properties (elongation to failure of 3000% with a corresponding strain rate sensitivity coefficient m of ≈0·6) were attained at 450°C and $\dot{\varepsilon}=1{\cdot}4 \times 10^{-2}\ s^{-1}$ in samples processed at 400°C to a total strain of ≈16. The alloy in this state had an average grain size of ≈2·6 μm and the recrystallisation fraction was about 90%. It was shown that the highest superplastic ductility appears in samples with more uniform microstructure containing the highest portion of high angle boundaries. It was established that the uniformity of structure and its stability under superplastic deformation is more important for achieving superior elongation to failure than the grain size if the latter varies from 0·5 to 2·6 μm.

Keywords: Superplasticity, Aluminium alloys, Equal channel angular extrusion, Ultrafine grain structure

Introduction

It is well known that Al–Li–Mg alloys are attractive materials for aerospace applications because of an excellent combination of low density, high strength and superior crack propagation resistance at ambient temperature in recrystallised condition.[1] In addition, these alloys with ultrafine grained structure exhibit high tensile ductilities associated with superplastic flow at intermediate temperatures.[2] In contrast, in unrecrystallised condition the Al–Li–Mg alloys show limited workability and poor service properties as a result of extensive localisation of plastic flow.[1,2] An important current objective is therefore to find a best way to produce ultrafine grain structure in these alloys. Traditional thermomechanical processing (TMP) consisting of cold or warm working and final recrystallisation annealing could not be applied to the Al–Li–Mg alloys because of poor workability of these alloys at low temperatures that led to a premature fracture under working conditions.[1,2]

It is known that the grain size in bulk billets of aluminium alloys may be significantly reduced by imposing an intense plastic strain through the process of equal channel angular extrusion (ECAE).[3–5] Aluminium alloys having micron or submicron scale grain sizes are capable to exhibit superior superplastic ductility at higher strain rates or lower temperatures that makes the utilisation of superplastic forming highly attractive. The basic requirements for these superplastic aluminium alloys is the development of a simple processing route providing the fabrication of bulk samples with ultrafine grained structure.[6–10] The fabrication of a nanoscale grain size in the Al–Li–Mg alloys through intense plastic straining at room temperature has no advantages as compared to the production of micrometer scale grains through an ECAE at intermediate temperature.[3,6,10] In addition, the bulk billets from these alloys with ultrafine grained structure could not be produced through ECAE at room temperature as a result of extensive cracking. Therefore, the intense plastic straining at elevated temperatures is highly suitable for the development of superplasticity in Al–Li–Mg alloys because of their enhanced workability at these conditions, which prevents cracking and facilitates the extrusion process.[6,10] However, it was recently shown in Refs. 11 and 12 that an increase in temperature of ECAE leads to an increase in grain size and an increased portion of low angle boundaries (LABs) in final structure that results in degradation of superplastic properties in conventional aluminium alloys.[2] At the same time ECAE at elevated temperatures enables an increase in the strain that can be imposed into less ductile materials such as Al–Li–Mg alloys that provide increased fraction of ultrafine grains.[2,11–15] It is expected that an increased portion of high angle boundaries (HABs) provides the enhancement of superplastic ductilities.[2,16]

[1]Institute for Metals Superplasticity Problems, Khalturina 39, Ufa 450001, Russia
[2]Ibaraki University, Research Center for Superplasticity, Hitachi, Ibaraki, Japan

*Corresponding author, email rustam@anrb.ru

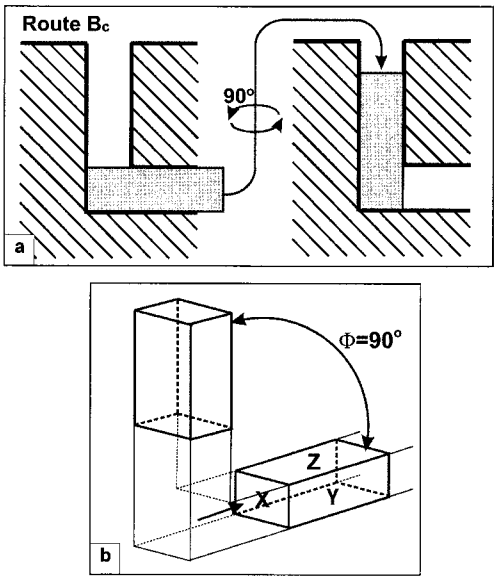

a the pressing route B_C; *b* ECAE processing

1 Schematic illustration

Accordingly, the present study was initiated to establish the optimal temperature of ECAE processing which has to provide the achievement of highest superplastic properties for an Al–Li–Mg–Sc alloy. This alloy was designated in the former Soviet Union as 1421 AA and denoted as 1421 Al hereon. To date there has been no attempt to evaluate the effect of microstructure evolved under ECAE processing on superplastic properties, because the significance of the total imposed strain and the temperature of ECAE processing on the subsequent ductilities attained in an Al–Li–Mg–Zr alloy was recently shown.[6] This paper is focused on examination of temperature effect of ECAE on superplastic properties in the 1421 Al.

Material and experimental procedure

The 1421 Al with a chemical composition of Al–2Li–4·1Mg–0·07Si–0·16Sc–0·08Fe–0·08Zr (wt-%) was manufactured by direct chill casting followed by a solution treatment at 460°C for 12 h. Bars with diameter 20 mm and length 100 mm were machined from the central part of the ingot parallel to the major direction. These rods were deformed by ECAE using an isothermal die at three temperatures

(i) to a total strain of ≈2 at 240°C (Route I)
(ii) to a total strain of ≈16 at 325°C (Route II)
(iii) to a total strain of ≈16 at 400°C (Route III).

The die with a circular internal cross-section and an 'L' shaped configuration with angles Φ and ψ equal to 90° and ≈1°, respectively, was used for the extrusion. Deformation through this die produced a strain of ≈1 on each passage. The temperatures of the rods and the die were almost the same; temperature accuracy was within ±5 K. The rods were repetitively pressed through the die with rotation by 90° around the extrusion axis in the same direction between each pressing, i.e. route B_C was used (Fig. 1*a*).[4,8] The shearing characteristics for this processing route in a tabular form were clearly presented in Fig. 6 in Ref. 8. The ram speed was about 2 mm s^{-1}. At 240°C, the samples were only pressed up to a total strain of ≈12, at which an extensive surface cracking started to occur resulted in sample fracture under further pressings. At $T \geqslant 325$°C, no surface defects were found at a total strain of ≈16.

Following ECAE, samples were sliced from the central area of the rods, the slicing plane was parallel to the extrusion direction and contained the extrusion direction (ED) and the transverse extrusion direction (ET) (Fig. 1*b*). That is, the deformed structure was characterised at the centre of the *Y* plane (Fig. 1 of Ref. 8).

Tensile specimens were machined parallel to the extrusion axis with gauge lengths of 6 mm and cross-sectional dimensions of $1{\cdot}5 \times 3$ mm^2. These samples were pulled to failure in air using an Instron universal testing machine (model 1185) operating at a constant cross-head velocity. Tension tests were performed at strain rates ranging from $1{\cdot}4 \times 10^{-5}$ to 1·4 s^{-1} in the temperature interval 300–500°C. Temperature accuracy was within ±2 K. Each sample was held at a testing temperature for about 30 min in order to reach thermal equilibrium. The values of the strain rate sensitivity ($m = d\ln\sigma/d\ln\dot{\varepsilon}$, where σ is flow stress and $\dot{\varepsilon}$ is strain rate) were determined by strain rate jump tests.[2,16] The magnitudes of elongation to failure were measured by using two scratches within gauge sections of samples.

Samples for metallographic examinations were annealed at $T = 170$°C for 4 h in order to decorate grain boundaries with secondary phase particles. These grain boundary particles were revealed by etching with standard Keller's reagent. Metallographic analysis was carried out using an Olympus BX60 and Neophot 32 optical microscope. The mean grain size was determined by the linear intersect method from measurements of more than 300 grains in longitudinal and transverse directions. Cavitations were measured in samples by optical microscopy using the standard point count technique. Other details of metallography observations and cavitation studies were reported previously.[18,19]

For TEM examinations, samples were thinned to about 0·2 mm. Discs of 3 mm diameter were cut and electropolished to perforation with a Tenupol 3 twinjet polishing unit using a 30% nitric acid solution in methanol at −30°C and 20 V. The thin foils were examined using a Jeol 2000EX electron microscope with a double tilt stage at an accelerating potential of 200 kV. Technique for estimation of lattice dislocation density was described in Ref. 17 in details.

Misorientations of (sub)grain boundaries were studied by electron backscattering diffraction (EBSD) analysis using a Jeol JSM 840 scanning electron microscope (SEM) fitted with automated EBSD pattern collection system provided by Oxford Instruments Ltd. HABs with misorientation over 15° and LABs with misorientation ranging from 2 to 15° were depicted in OIMDefine OIM on first mention maps as bold and thin lines, respectively. Misorientations less than 2° therefore were excluded from the EBSD data.

Experimental results

Microstructure after ECAE

Representative misorientation maps, distribution of misorientations and typical TEM structures are shown in Figs. 2–4 for the 1421 Al subjected to three different

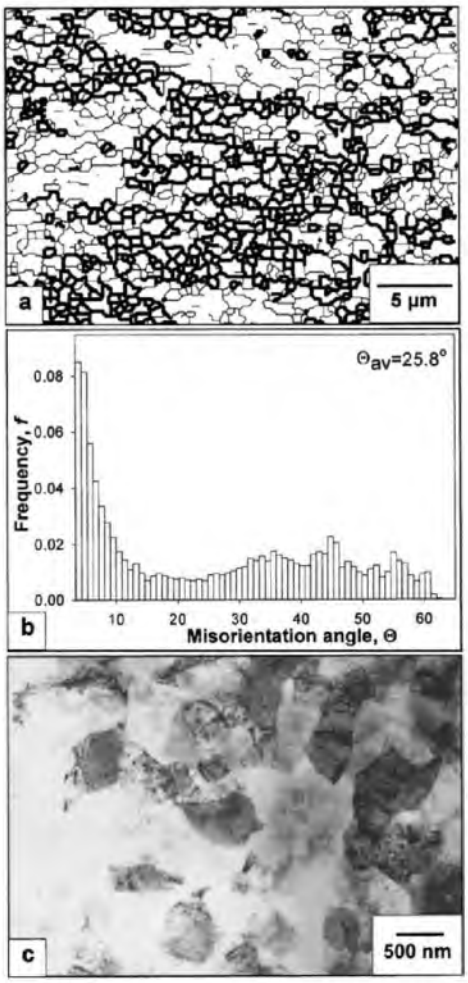

a misorientation map; *b* distribution of misorientation; *c* TEM structure

2 Typical microstructures of the 1421 Al processed via route I

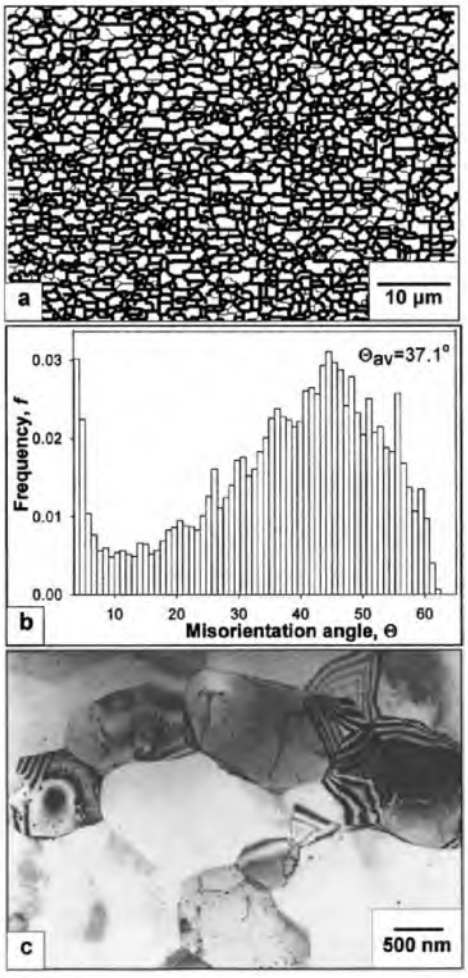

a misorientation map; *b* distribution of misorientation; *c* TEM structure

3 Typical microstructures of the 1421 Al processed via route II

routes of ECAE. Volume fraction of recrystallised grains, average misorientations, average size of grains and population of HABs are summarised in Table 1.

After ECAE processing at 240°C, the deformed structure is inhomogeneous; two structural components could be distinguished. Areas of eqiaxed grains with an average size of ≈0·6 μm (Fig. 2*a*) alternates with a structure consisting of elongated subgrains (longitudinal size is ≈0·7 μm) aligned along the shear direction (Fig. 2*a* and *c*). Increased dislocation density of $1{\cdot}4 \times 10^{14}$ m^{-2} was found within these subgrains. The unrecrystallised fraction is about 40%. Despite the 60% population of HABs the number of true grains entirely outlined by HABs is not so high (Fig. 2*b*, Table 1). In general, crystallites bounded partly by LABs and partly by HABs are dominant (Fig. 2*a*). As a result, distribution of misorientations is distinctly bimodal (Fig. 2*b*). Two peaks associated with LABs and HABs can be distinguished in the misorientation histograms. Low angle misorientations of less than 4° associate with LABs located within the unrecrystallised areas and high angle misorientations are attributed to HABs placed within the recrystallised areas (Fig. 2*a* and *b*). An average misorientation of 26° and the population of HABs of ≈57% suggests uncompleted transformation of LABs into HABs during ECAE at 240°C.[5] Most deformation induced HABs exhibit specific extinction contrast attributed to a very high density of lattice grain boundary dislocations over 10^8 m^{-1} (Fig. 2*c*) suggesting their non-equilibrium state.[20] It is worth noting that a relatively low density of lattice dislocation (≈$2{\cdot}1 \times 10^{13}$ m^{-2}) was observed within interiors of recrystallised grains.

Table 1 Effect of ECAE temperature on grain size *d*, volume fraction of high angle boundaries V_{HAB}, average misorientation of deformation induced boundaries Θ_{av}, and volume fraction of recrystallised grains V_{recr}

Route	I	II	III
d, μm	0·6	0·8	2·6
V_{HAB}, %	57·2	87·9	91·4
Θ_{av}, degr.	25·8	37·1	38·1
V_{recr}, %	62	90	92

In contrast, ECAE processing through routes II and III resulted in almost fully recrystallised structure (Figs. 3 and 4, Table 1). A well defined maximum on misorientation histograms attributed to HABs appears (Figs. 3*b* and 4*b*). True recrystallised grains entirely delimited by HABs are highly dominant (Figs. 3*a* and 4*a*). Grain boundaries exhibit a well defined extinction

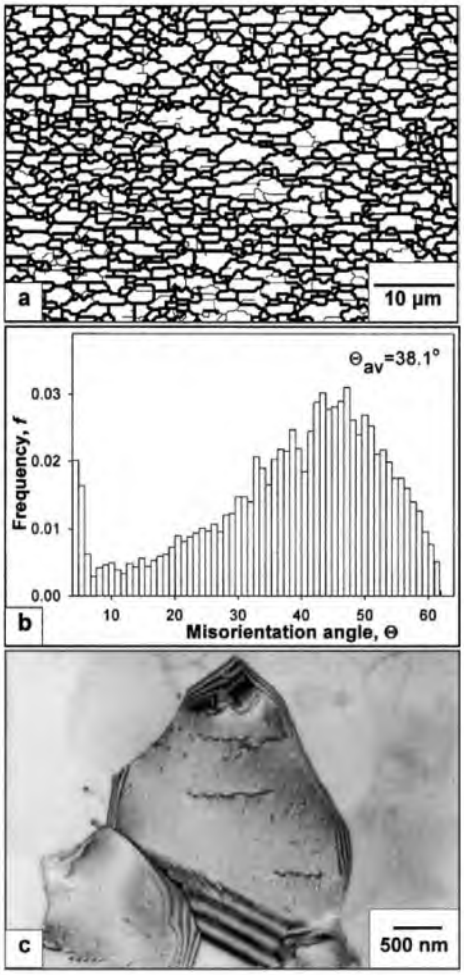

a misorientation map; *b* distribution of misorientation; *c* TEM structure

4 Typical microstructures of the 1421 Al processed via route III

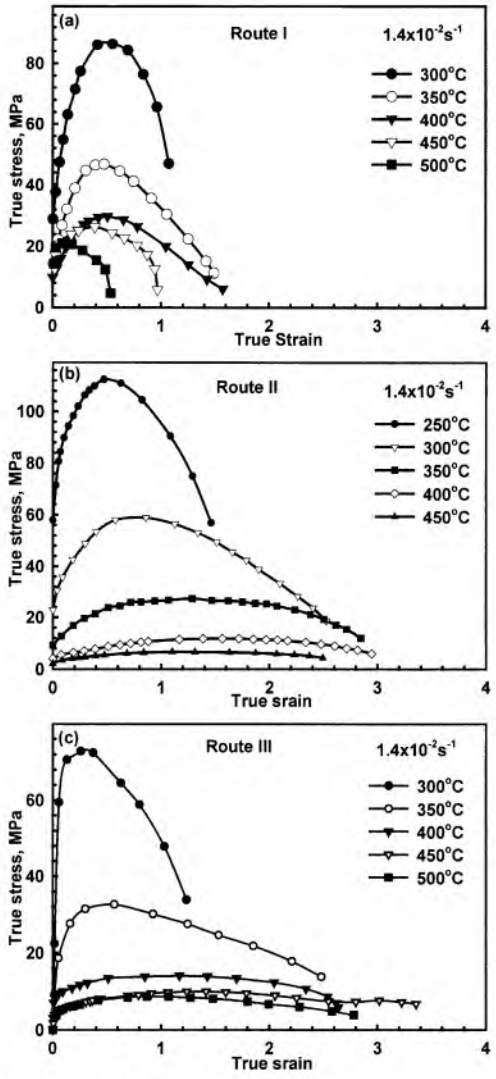

a 240°C; *b* 325°C; *c* 400°C

5 Typical true stress–true stain curves for 1421 Al subjected to ECAE

contrast (Figs. 3*c* and 4*c*) suggesting their equilibrium state. It is seen that an increase in temperature of ECAE processing from 325 to 400°C leads to an increase in average grain size from about 0·8 to 2·6 μm, the portion of HABs increases from about 88 to 91% (Table 1) and the average density of lattice dislocation within recrystallised grains decreases from 7×10^{12} to 10^{11} m^{-2}. Therefore, at $T\geqslant325$°C, increasing temperature of ECAE processing leads mainly to increased grain size and decreased lattice dislocation density.

Notably it was recently established that as evidence of ultrafine grained structure the fraction of HABs is greater than 65–75%.[5] There exists a strong correlation between the portion of HABs in deformed structure and the uniformity of microstructure evolved during subsequent static annealing.[21] When HAB%<62, discontinuous static recrystallisation occurs resulting in microstructural instability, which allows a non-uniform microstructure to evolve.[21] When HAB%>64, the microstructure becomes progressively stable against catastrophic growth of grains bounded by HABs a therefore a roughly uniform microstructure is retained under static annealing.[21] It is expected, therefore, that in the 1421 Al processed through routes II and III the fully recrystallised structure consisting of fine grains will remain stable through the superplastic deformation process. In contrast, abnormal grain growth is expected to occur in the partially recrystallised structure evolved during ECAE at 240°C.

Mechanical properties

The typical true stress–true strains (σ–ε) for the 1421 Al processed through different routes at an initial strain rate of $1{\cdot}4\times10^{-2}$ s^{-1} and temperatures ranging from 300 to 500°C are shown in Fig. 5. A well defined stress peak is observed after processing through route I (Fig. 5*a*). Extensive strain hardening takes place initially. At $T\leqslant350$°C, after reaching a maximum stress, the flow stress sharply drops resulting in premature fracture caused by unstable plastic flow (Fig. 6*a*).[16] At $T\geqslant400$°C, the pseudo-brittle fracture was found (Fig. 6*a*).[16] An increase in temperature leads to merely decreasing flow stress; the shape of the σ–ε curves of the samples processed through route I remains essentially unchanged.

The samples processed through routes II and III exhibit low strain hardening. After reaching a maximum stress, the flow stress continuously decreases until failure (Fig. 5*b* and *c*). At $T\leqslant350$°C, the samples processed

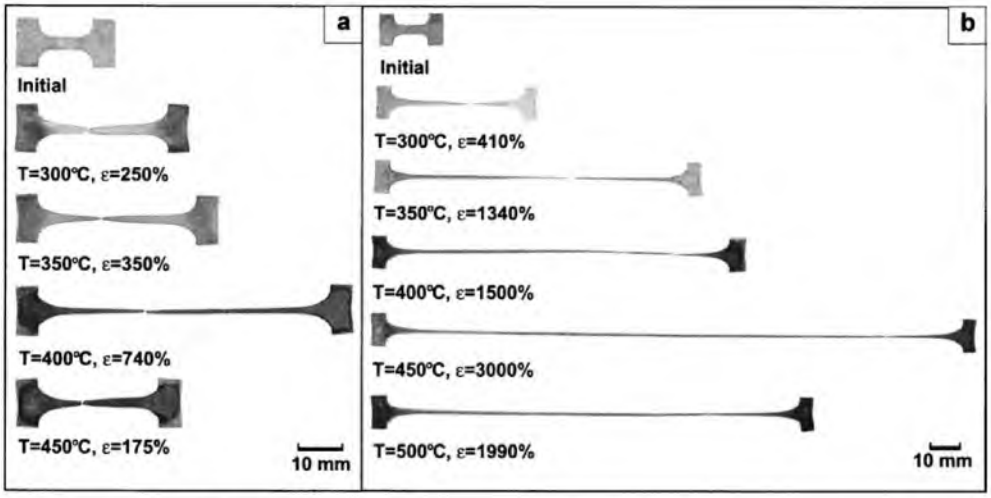

a at 240°C for 12 passes; *b* at 400°C for 16 passes

6 Shadowgraphs of the fracture in two different states of the 1421 Al after ECAE

through route III demonstrate increased initial strain hardening; the stress peak is attained at low strains and a stronger strain softening was observed comparing with the samples processed through route II. Fracture owing to unstable plastic flow takes place in the samples processed through route III at 300°C (Fig. 6*b*). At $T \geqslant 350$°C, a very uniform deformation visible in gauge length occurs in these samples. The steady state flow occurs at $\dot{\varepsilon}=1{\cdot}4\times10^{-2}$ s^{-1} in the temperature interval 400–500°C, which corresponds with superior ductility (Fig. 5*c*). Notably, the samples processed through route II demonstrated the pseudo-brittle fracture in the temperature interval 300–500°C.[10] Apparent steady state flow could be distinguished at $T \geqslant 350$°C and $\dot{\varepsilon} \leqslant 1{\cdot}4\times10^{-2}$ s^{-1}.[10] An increase in temperature (Fig. 5*b* and *c*) or a decrease in strain rate leads to a shift of the peak stress towards higher strains and a reducing strain hardening coefficient.

Figure 7 shows plots of flow stresses σ taken at a true strain of $\approx$0·4 as a function of strain rate. The variation of strain rate sensitivity coefficient m and elongation to failure δ with strain at fixed temperatures of 300 and 400°C are presented in Figs. 8 and 9, respectively. The σ–$\dot{\varepsilon}$ curves of all of the states of the 1421 Al show evidence of a sigmoidal shape with the maximum coefficient m at a strain rates over 10^{-2} s^{-1} (Fig. 8).[10] It is seen that the 1421 Al processed through route I exhibits the highest flow stress and low ductility corresponding with the lowest m values (Figs. 7–9). Samples processed through route II show the lowest flow stress (Fig. 7). The m values of samples processed through routes II and III are essentially the same (Fig. 8). It is worth noting that at 300°C, in the samples processed through route II, the optimal strain rate for superplasticity at which the highest m value appears is higher by a factor of two than that for the samples processed through route III. In contrast, at 400°C, the optimal strain rate for superplasticity ($\dot{\varepsilon}=1{\cdot}4\times10^{-2}$ s^{-1}) is similar for all of the states of the 1421 Al. Maximums of elongation to failure also appear at this strain rate (Fig. 9*a*); the sample processed through route II exhibits the highest ductility of $\approx$2100%. At 450°C, a maximum elongation to failure of $\approx$3000% corresponding with

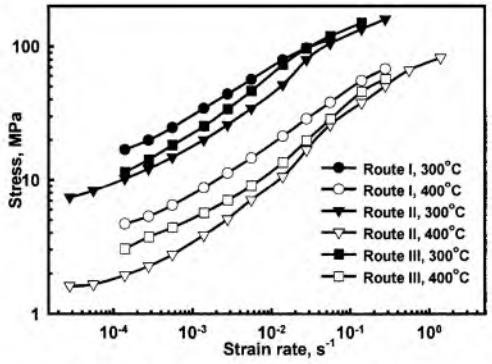

7 Variation of a flow stress σ taken at $\varepsilon\approx$0·4 with strain rate

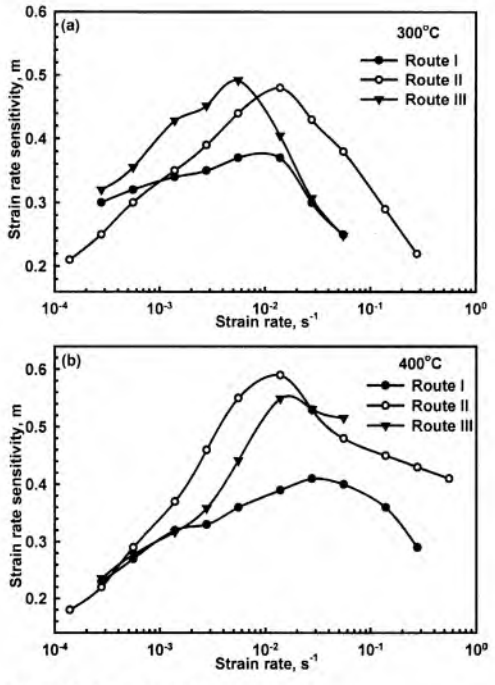

a at 300°C; *b* at 400°C

8 The coefficient of strain rate sensitivity *m* as a function of strain rate

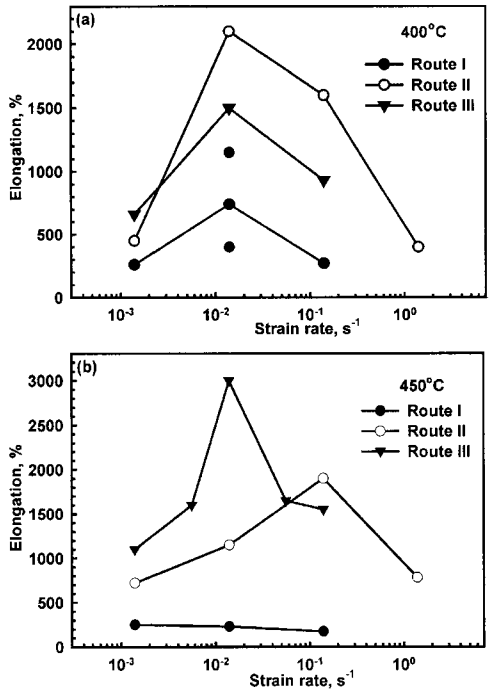

a at 400°C; *b* at 450°C

9 Elongation to failure as a function of strain rate

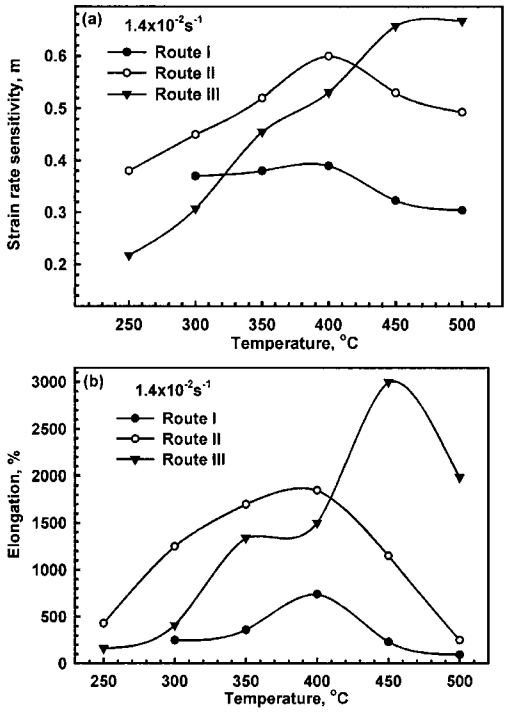

a on strain rate sensitivity m; *b* on elongation to failure δ

10 Effect of temperature

m=0·6 was demonstrated by a sample processed through route III at $\dot{\varepsilon}=1{\cdot}4\times10^{-2}\ s^{-1}$; the highest ductility ($\delta\approx1990\%$) of samples processed through route II appeared at $\dot{\varepsilon}=1{\cdot}4\times10^{-1}\ s^{-1}$ (Fig. 9*b*). Therefore, at temperatures of 400 and 450°C, the highest superplastic ductilities were demonstrated by the samples processed through routes II and III, respectively.

The m value and elongation to failure δ are plotted as a function of temperature at a strain rate of $1{\cdot}4\times10^{-2}\ s^{-1}$ in Fig. 10. It is seen that all of the states of the 1421 Al exhibit well defined maximums of elongation to failure (Fig. 10*b*) despite the fact that the m value in state III tends to increase with increasing temperature (Fig. 10*a*). Samples processed through routes I and II show the highest m values at a similar temperature of 400°C, at which the highest superplastic ductilities were found. At $T\leqslant400$°C, in all of the states of the 1421 Al an increase in temperature results in increasing δ values. At higher temperatures, reduced δ values are observed in the samples processed through routes I and II (Fig. 10*b*). The highest elongation to failure of ≈3000% was attained in the 1421 Al processed through route III at 450°C. Upon further increase in temperature the δ value tends to decrease. Therefore, at $T\leqslant400$°C, highest superplastic ductility was attained in the samples processed through route II (Fig. 10*b*). At $T>400$°C, the samples processed through route III exhibit the highest total elongation. Notably samples processed through routes II and III show wide temperature domains of superior superplasticity in which $\delta\geqslant1000\%$. The extension of this domain (150°C) is similar for these two states of 1421 Al. However, the temperature domain of superior superplasticity of the samples processed through route III (350–500°C) is shifted towards elevated temperatures compared with that for route II (300–450°C) (Fig. 10*b*). The 1421 Al processed through route I exhibits moderate ductility (<500%) at all temperatures except for 400°C at which the highest elongation to failure of ≈740% with a corresponding m value of 0·4 was achieved (Fig. 10). However, the reproducibility of this result is low. Three samples pulled to failure at this temperature and strain rate showed a great scattering in elongation to failure ranging from 440 to 1150% (Fig. 9*a*).

The superplastic properties, therefore, are superior after ECAE processing at $T\geqslant325$°C and the 1421 Al processed through route I shows moderate superplastic properties.

Table 2 Average grain sizes of 1421 Al (route I)*

T, °C	Local strain in the area examined (the period of equivalent exposure time, h)	L_s, μm†	L_d, μm‡	Aspect ratio	V, %
350	1·6 (0·58)	1·7	5·7/2·7	2·11	8·2
400	(0·66)	1·6	6·0/3·6	1·67	8·7
450	(0·56)	7·8	10·5/6·5	1·62	12·1
500	(0·28)	9·9	18·4/10·1	1·82	8·8

* After static (grip section) L_s and dynamic (gauge section) L_d annealing, grain aspect ratio AR and porosity volume fraction V in gauge sections for the samples processed via route I and pulled up to failure at a strain rate of $1{\cdot}4\times10^{-2}\ s^{-1}$ and different temperatures. The true strain in the gauge section and the period of equivalent time of static annealing (in hours) are also indicated

† TEM data

‡ Numerator and denominator are grain sizes measured in the longitudinal and transverse directions, respectively

Microstructural evolution under superplastic conditions

The microstructural evolution of the 1421 Al processed through different routes was examined under both static (grip section) and dynamic (gauge section) annealing at an initial strain rate of $1{\cdot}4 \times 10^{-2}$ s^{-1} in the temperature range 350–500°C. Grain sizes observed after static annealing L_s, dynamic annealing L_d and grain aspect ratio AR, defined as the ratio of the grain dimension in the tension direction to that in the transverse direction, are summarised in Tables 2–4. It is worth noting that only grains having an equiaxed shape were taken into account to determine the average grain size within grip section of the samples pulled to failure. In the 1421 Al processed through route I a significant growth of ultrafine grains occurs at $T>400$°C (Table 2). However, the unrecrystallised fraction (≈36%) remains essentially unchanged up to 450°C (Fig. 11*a*). At 500°C, an extensive grain growth results in coarse grain structure (Fig. 11*b*). Deformed structure in samples processed through routes II and III exhibits high stability under static annealing at $T\leqslant 400$°C and $T\leqslant 450$°C, respectively, as was expected. An extensive static grain growth starts to occur in the samples processed through routes II and III at higher temperatures (Tables 3 and 4). In the 1421 Al processed through route II, the transition from slow grain growth in a fine grained structure at $T\leqslant 450$°C to an extensive grain growth at higher temperatures even results in a negative temperature dependence of flow stress (Fig. 5*b*). A slow static grain growth takes place in the state III at $T>450$°C (Table 4). Notably, in the samples processed through routes II and III an extensive growth of unrecrystallised grains starts at a temperature of 450°C (Tables 3 and 4; Fig. 11*c* and Fig. 9*d* from Ref. 10). Unrecrystallised volume fraction attain ≈30% and ≈20%, respectively.[10] In summary, the onset of remarkable growth of ultrafine grains takes place at $T\geqslant 400$°C in the samples processed through routes I and at temperatures over 450°C in the 1421 Al processed through routes II and III. It is reasonable to conclude that the deformed structure evolved under route III showed highest stability under static annealing.

Superplastic deformation leads to a remarkable strain induced grain growth in all of the states of the 1421 Al (Figs. 12 and 13). Notably the micrographs presented in Fig. 12 and Fig. 13*b* were taken from areas in the vicinity of the fracture surface. The other micrographs were obtained from areas located at points over 10 mm from the fracture tip. In the samples processed through route I the coarse elongated grains are retained under dynamic annealing at all temperatures except for 400°C, at which the uniform fine grain structure is evolved (Fig. 12*a*). At $T<400$°C, the average value AR>2·1 calculated for recrystallised grains is indicative for the decreased contribution of grain boundary sliding (GBS) to total elongation.[2,16] At $T\geqslant 450$°C, an extensive growth of fine grains hinders GBS (Fig. 12*b*). Grain growth and increasing AR with strain at temperatures over and less than 400°C, respectively, are expected to reduce the likelihood of GBS and therefore superplastic ductility in the samples processed through route I. At 400°C, dynamic recrystallisation (DRX) resulting in grain refinement within unrecrystallised areas provides the achievement of superplastic ductilities over 1000%. It is apparent that a great scattering in superplastic ductility associates with variation in fraction of unrecrystallised grains in initial samples. Superior ductility appears when the volume fraction of unrecrystallised grains is low and DRX can provide the formation of homogeneous microstructure at initial stage of superplastic deformation. If unrecrystallised fraction is high these grains retain under dynamic annealing restricting ductility.

Slow grain growth under superplastic deformation occurs in samples processed through routes II and III at $T\leqslant 450$°C (Fig. 10 from Ref. 10 and Fig. 13). Notably, at 400°C, the final grain size after superplastic deformation in the samples processed through route II is lower than that in the samples processed through route III (Tables 3 and 4). At $T\geqslant 450$°C, the resulting grain sizes in the samples processed through routes II and III are almost the same (Tables 3 and 4). In addition, the deformed structure evolved during superplastic flow in the samples processed through route III is more uniform (Fig. 13*a*) than that in the samples processed through route II (Fig. 10*c* from Ref. 10) because of extensive grain refinement within unrecrystallised grains. At $T>400$°C, the smallest AR values ($\leqslant 1{\cdot}5$), which suggest a high contribution of GBS to the total elongation, were found in the samples processed through route III (Tables 4).[2,16]

Metallographic observation of superplastically deformed samples showed that fine cavities exhibiting equiaxed shape suggesting diffusion controlled growth play unimportant role in the fracture of the 1421 Al subjected to different routes of ECAE processing.[10,16] The formation of crack-like cavities exhibiting irregular and jagged shape was observed within highly elongated areas of unrecrystallised structure in state I (Fig. 12) and within areas of relatively coarse grains having equiaxed shape in the samples processed through routes II and III (Fig. 13*b*).[10] The shape of these voids suggests the plasticity controlled cavity growth owing to

Table 3 Average grain sizes of the 1421 Al (route II)*

T, °C	Local strain in the area examined (the period of equivalent exposure time, h)	L_s, μm†	L_d, μm‡	Aspect ratio	*V*, %
350	2·3 (0·87)	0·9	2·7/2·3	1·17	0·4
400	(0·9)	1·2	3·9/3·2	1·22	0·3
450	(0·75)	2·3	7·1/4·7	1·51	2
500	(0·28)	7·3	10·2/7·0	1·46	3·7

* After static (grip section) L_s and dynamic (gauge section) L_d annealing, grain aspect ratio AR and porosity volume fraction *V* in gauge sections for the samples processed via route II and pulled up to failure at a strain rate of $1{\cdot}4 \times 10^{-2}$ s^{-1} and different temperatures. The true strain in the gauge section and the period of equivalent time of static annealing (in hours) are also indicated

† TEM data

‡ Numerator and denominator are grain sizes measured in the longitudinal and transverse directions, respectively

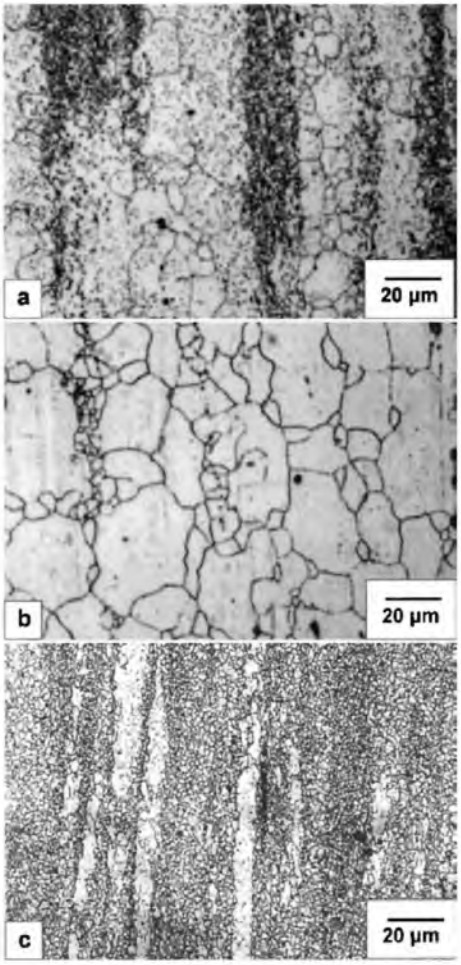

a, *b* via route I; *c* via route III; at *a*, *c* 450°C; *b* 500°C

11 Effect of static annealing on microstructures of samples processed

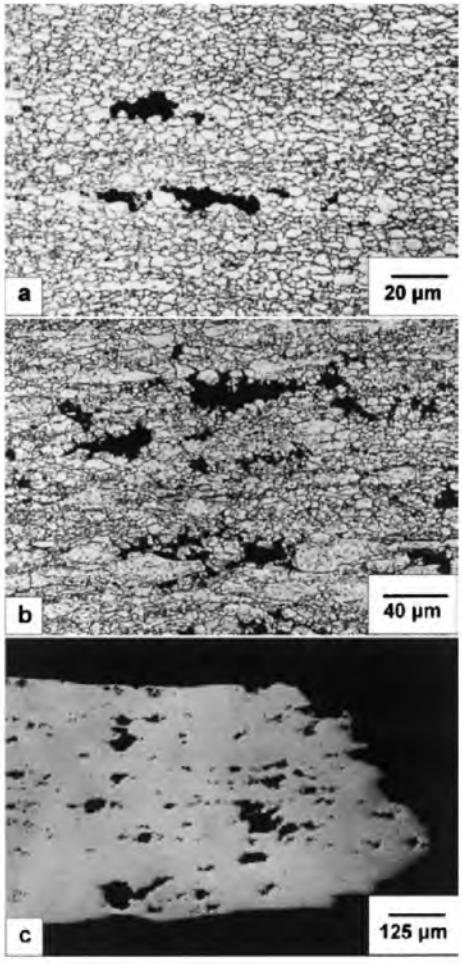

a 400°C; *b*, *c* 450°C

12 Microstructure after superplastic deformation at $1{\cdot}4 \times 10^{-2}$ s^{-1} of samples processed via route I

non-uniformity of GBS and incompatibility of plastic deformation between areas of equiaxed fine grains and areas of highly elongated grains.[16,17] It is apparent that extensive void coalescence takes place in the unrecrystallised areas resulting in the cavity size being similar to the size of these areas (Fig. 12*b*). Notably, such cavitation is unacceptable for a commercial alloy used as a structural material. Therefore, the forming limit for superplastic forming (SPF) of the 1421 Al will be limited by the formation of these large voids. From this point of view, the samples processed through routes II and III can be deformed up to elongations over 1000%, whereas the useful ductility of the samples produced through route I will be less than 500%.

In the samples processed through route I the size of these voids is larger. Fracture occurs through crack propagation between these coarse cavities at an angle of $\approx 45^{\circ}$ to the tension axis (Fig. 12*c*). In the samples processed through routes II and III the pseudo-brittle fracture occurs as a result of cavity interlinkage resulted from the formation of cavity chains in the tension direction near residual unrecrystallised grains or coarse grains exhibiting equiaxed shape. As a result, the fracture tips in the states II and III locate at angle of 90° to the tension axis (Fig. 6). Therefore, the premature fracture in the 1421 Al is attributed to unrecrystallised grains, which retained under superplastic deformation, and abnormal growth of separate

Table 4 Average grain sizes of the 1421 Al (route III)

T, °C	Local strain in the area examined (the period of equivalent exposure time, h)	L_s, μm†	L_d, μm‡	Aspect ratio	*V*, %
350	2·3 (0·75)	2·6	3·1/2·0	1·55	0·6
400	(0·8)	2·6	6·0/4·4	1·36	0·4
450	(1·1)	2·9	7·5/5·5	1·36	1·1
500	(0·9)	4·1	10·1/8·4	1·20	3·1

* After static (grip section) L_s and dynamic (gauge section) L_d annealing, grain aspect ratio AR and porosity volume fraction *V* in gauge sections for the samples processed via route II and pulled up to failure at a strain rate of $1{\cdot}4 \times 10^{-2}$ s^{-1} and different temperatures. The true strain in the gauge section and the period of equivalent time of static annealing (in hours) are also indicated

† TEM data

‡ Numerator and denominator are grain sizes measured in the longitudinal and transverse directions, respectively

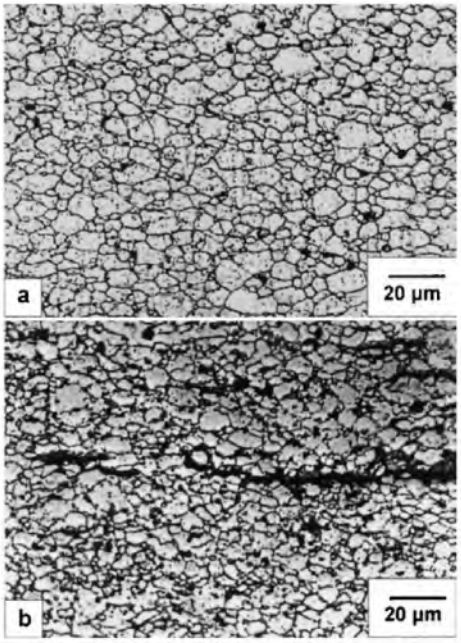

13 Microstructure after superplastic deformation at $1{\cdot}4 \times 10^{-2}\ s^{-1}$ of samples processed via route III at 450°C

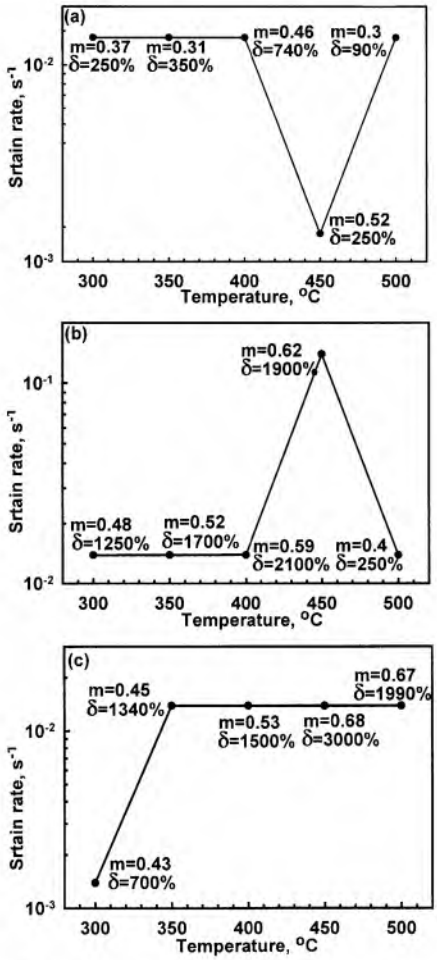

Samples processed via: *a* route I; *b* route II; *c* route III

14 Temperature dependence of the strain rate at which the highest value of strain rate sensitivity was observed

fine grains under dynamic annealing. Therefore, instability and heterogeneous of deformed structure limits the superplastic ductility under the optimal superplastic conditions. It is obvious that a decrease in the volume fraction of unrecrystallised areas because of DRX during superplastic deformation, and a uniform growth of fine grains are necessary conditions for achieving superior ductilities in the 1421 Al that can be used in SPF techniques.

Discussion

The present study clearly demonstrates that the highest reduction in grain size by ECAE processing at low temperature does not guarantee the achievement of the highest superplastic properties in the 1421 Al. It is seen that the subsequent superplastic properties are highest when a processing route provides the formation of more uniform structure.

Effect of structure uniformity on superplastic properties

Inspection of the experimental data shows that the 1421 Al subjected to ECAE demonstrates superplastic behaviour in two distinctly different microstructure conditions.[16,22–24] The 1421 Al processed through routes II and III exhibits superplastic behaviour in a recrystallised condition whereas the alloy processed through route I shows superplasticity in a partially recrystallised condition.[25] It is seen that superplastic properties of the 1421 Al in the recrystallised condition are higher than that in the partially recrystallised condition. In addition, in the samples processed through routes II and III the temperature domain of superplasticity is significantly larger than that in the samples processed through route I, which demonstrates high superplastic properties at 400°C owing to DRX.[16,22–24] It is apparent that in the temperature interval 400–450°C the occurrence of DRX within unrecrystallised areas provides the formation of fine grains here and decreases cavitation. Unrecrystallised areas are eliminated because of DRX that highly increase the plasticity resource. Superior superplastic ductility in the 1421 Al corresponds with high uniformity of initial structure evolved during static annealing. This is why the highest ductility appeared in the samples processed through route III. Therefore, the main requirement to ECAE processing of the 1421 Al to attain high superplastic ductility is the formation of homogeneous microstructure.

Effect of grain size on superplastic properties

The strain rate in superplasticity, $\dot{\varepsilon}$, generally obeys the following relationship

$$\dot{\varepsilon} = A\,\frac{DGb}{kT}\left(\frac{b}{d}\right)^{p}\left(\frac{\sigma}{G}\right)^{2} \qquad (1)$$

where A is a dimensionless constant, b is the Burgers vector, d is the grain size, σ is the applied stress, G is the shear modulus, k is Boltzmann's constant, D is the grain boundary diffusion coefficient defining the temperature dependence of the strain rate at constant stress and structure, T is the absolute temperature and p is the exponent of the inverse grain size ranging from 2 to 3.[2,16] Because the strain rate in superplasticity is inversely proportional to the square or cube of the grain

size, one can therefore expect that the superplastic domain is displaced to faster strain rates or lower temperatures when the grain size of a material is reduced. However, temperature dependencies of the strain rate at which the highest values of strain rate sensitivity appear, as summarised in Fig. 14, do not support this conclusion.

It is seen that the optimal strain rate of superplastic deformation is similar for all of the states of the 1421 Al in the temperature interval 350–400°C; the variation in initial grain size from 0·5 to 2·6 μm affects insignificantly the total elongation. The highest superplastic ductility appears in the samples processed through route III despite the grain size being higher than that in the samples processed through route II. This clearly demonstrates that merely producing a fine grain size is not in itself sufficient to guarantee achieving highest superplastic ductility, because the grain size needs to remain stable throughout superplastic deformation.[16] In the samples processed through route III the slow and uniform grain growth under dynamic annealing prevents the formation of large voids with irregular shape as a result of non-uniform grain boundary sliding.[16] As a result, this material showed extraordinary plasticity. Highest superplastic ductilities were attained when the strain enhanced grain growth under superplastic deformation resulted in smallest grain size. At $T \leqslant 400$°C, the slowest strain induced grain growth takes place in the samples processed through route II and, as a result, this state of 1421 Al exhibits highest total elongations. At 450°C, normal strain induced grain growth in the samples processed through route III results in more uniform structure. The highest ductility attained in these samples is significantly larger than that in the samples processed through route II.

Optimal temperature of ECAE processing

Therefore, the working at elevated temperatures not only facilitates the process of ECAE, but also provides the achievement of the enhanced properties. At $T \geqslant 325$°C, the 1421 Al has excellent workability that prevents surface cracking making the ECAE easier because of lower flow stress. ECAE processing of the 1421 Al containing a significant fraction of coherent nanoscale dispersoids at elevated temperatures provides the formation of highly uniform structure.[10]

The highest superplastic ductility was achieved in the 1421 Al with the highest grain size of ≈2·6 μm owing to most uniform structure. It is apparent that route III looks is the optimal one for achieving high strain rate superplasticity in the 1421 Al. However, the superplastic deformation at lower temperatures provides reducing surface oxidation and preventing depletion of the alloying elements in Al–Li alloys.[26,27] From this point of view the temperature of 325°C can be considered as the optimal temperature of ECAE for producing superplastic products from the 1421 Al. The 1421 Al with grain size of 0·8 μm exhibits superior superplastic ductilities at $T \leqslant 350$°C, at which width of the surface Li depletion layer is less than 11 μm.[26] The plasticity resource and very high optimal strain rate of superplastic deformation ($\dot{\varepsilon} = 1{\cdot}4 \times 10^{-1}$ s^{-1}) at $T > 400$°C of the 1421 Al processed through route II make this material highly attractive for commercial superplastic forming.

Summary and conclusions

1. ECAE processing at three different temperatures was applied to the Al–Li–Mg–Sc alloy to produce ultrafine grained structure. It was shown that the ECAE processing at 240°C to a total strain of about 12 resulted in partially recrystallised structure with an average size of fine grains of ≈0·6 μm. The ECAE processing at 325 and 400°C up to a total strain of ≈16 provided the formation of almost fully recrystallised structure with average grain sizes of ≈0·8 and ≈2·6 μm, respectively.

2. All of the states of the 1421 Al exhibit high strain rate superplasticity. The highest total elongation to failure of about 3000% with corresponding strain rate sensitivity of 0·6 was recorded at 450°C and strain rate of $1{\cdot}4 \times 10^{-2}$ s^{-1} for the 1421 Al subjected to ECAE at 400°C.

3. Ultrafine grained structure produced by ECAE showed high stability under both static and dynamic conditions at $T \leqslant 450$°C. Static growth of unrecrystallised areas resulted in inhomogeneous structure reducing superplastic ductilities.

4. At $T \geqslant 400$°C, dynamic recrystallisation occurs in the 1421 Al resulting in the elimination of unrecrystallised areas that highly increases superplastic ductility.

5. It was shown that cavitation taking place within unrecrystallised areas and near coarse growing grains leads to premature fracture under high strain rate superplasticity.

Acknowledgements

This paper was supported, in part, by the International Science and Technology Centre under Project no.2011 and Japan Light Metal Educational Foundation.

References

1. I. N. Fridlyander: *Met. Sci. Heat Treat.*, 2001, **1**, 5–9.
2. O. A. Kaibyshev: 'Superplasticity of alloys, intermetallides, and ceramics'; 1992, Berlin, SpringerVerlag.
3. R. Z. Valiev, R. K. Islamgaliev and I. V. Alexandrov: *Progr. Mater. Sci.*, 2000, **45**, 103–189.
4. S. Ferrasse, V. Segal, K. Hartwig and R. Goforth: *Metall. Mater. Trans.*, 1997, **28A**, 1047–1057.
5. F. J. Humphreys, P. B. Prangnell, J. R. Bowen, A. Gholinia and C. Harris: *Phil. Trans. R. Soc. Lond.*, 1999, **357A**, 1663–1681.
6. S. Lee, P. B. Berbon, M. Furukawa, Z. Horita, M. Nemoto, N. K. Tsenev, R. Z. Valiev and T. G. Langdon: *Mater. Sci. Eng.*, 1999, **A272**, 63–72.
7. R. Islamgaliev, N. Yunusova, R. Valiev, N. Tsenev, V. Perevezentsev and T. G. Langdon: *Scr. Mater.*, 2003, **49**, 467–472.
8. M. Furukawa, Z. Horita, M. Nemoto and T. G. Langdon: *Mater. Sci. Technol.*, 2000, **16**, 1330–1333.
9. F. Musin, R. Kaibyshev, Y. Motohashi and G. Itoh: *Scr. Mater.*, 2004, **50**, 511–516.
10. F. Musin, R. Kaibyshev, Y. Motohashi, T. Sakuma and G. Itoh: *Mater. Trans.*, 2002, **43**, 2370–2377.
11. A. Yamashita, D. Yamaguchi, Z. Horita and T. G. Langdon: *Mater. Sci. Eng. A*, 2000, **287**, 100–106.
12. Y. C. Chen, Y. Y. Huang, C. P. Chang and P. W. Kao: *Acta Mater.*, 2003, **51**, 2005–2015.
13. A. Goloborodko, O. Sitdikov, T. Sakai, R. Kaibyshev and H. Miura: *Mater. Trans.*, 2003, **44**, 766–774.
14. A. Goloborodko, O. Sitdikov, R. Kaibyshev, H. Miura and T. Sakai: *Mater. Sci. Eng. A*, 2004, **381**, 121–128.
15. S. Komura, M. Furukawa, Z. Horita, M. Nemoto and T. G. Langdon: *Mater. Sci. Eng.*, 2001, **A297**, 111–118.
16. J. Pilling and N. Ridley: 'Superplasticity in crystalline solids', 214; 1989, London, The Institute of Metals.
17. R. Kaibyshev, F. Musin, D. R. Lesuer and T. G. Nieh: *Mater. Sci. Eng.*, 2003, **342**, 169–177.

18. R. Kaibyshev, F. Musin, D. Gromov, T. G. Nieh and D. R. Lesuer: *Mater. Sci. Technol.*, 2003, **19**, 483–490.
19. R. Kaibyshev, T. Sakai, I. Nikulin, F. Musin and A. Goloborodko: *Mater. Sci. Technol.*, 2003, **19**, 1491–1497.
20. M. Mabuchi, K. Ameyama, H. Iwasaki and K. Higashi: *Acta Mater.*, 1999, **47**, 2047–2057.
21. H. Jazaeri and F.J. Humphreys: *Acta Mater.*, 2004, **52**, 3251–3262.
22. T. G. Nieh, L. M Hsiung, J. Wadsworth and R. Kaibyshev: *Acta Mater.*, 1998, **46**, 2789–2800.
23. Q. Liu, H. Huang, M. Yao and J.Yang: *Acta Metall. Mater.*, 1992, **40**, 1753–1762.
24. F. J. Humphreys and M. Hatherley: 'Recrystallization and related annealing phenomena', 392; 1996, Oxford, Pergamon Press.
25. R. Kaibyshev, A. Goloborodko, F. Musin, I. Nikulin and T.Sakai: *Mater. Trans.*, 2002, **43**, 2408–2414.
26. J. M. Pafazian, R. L. Schulte and P. N. Adler: *Metall. Mater. Trans. A*, 1986, **17A**, 635.
27. H. P. Pu, F. C. Liu and J. C. Huang: *Metall. Mater. Trans.*, 1995, **26A**, 1153–1166.